FLIGHT TEST RESULTS AT TRANSONIC REGION ON SUPERSONIC EXPERIMENTAL AIRPLANE (NEXST-1)

Dong-Youn Kwak*, Hiroaki ISHIKAWA, Kenji YOSHIDA***
***Japan Aerospace Exploration Agency, **Sankou Soft Co. Ltd.**

Keywords: *flight test, transonic, aerodynamics, CFD*

Abstract

A supersonic flight test was performed using a small scaled experimental airplane (NEXST-1) to demonstrate the aerodynamic design technology for the next generation SST. Aerodynamic forces at high Reynolds number and Mach 0.6-2.0 can be obtained from the flight test. Aerodynamic data at the transonic region were validated from comparing with flight test, CFD analysis and wind tunnel tests. When the CFD results compare with flight test results at high Reynolds number conditions, difference of the drag component was observed at both results. However, similar trend were obtained at CFD and flight test results at Mach number from 0.8 to 1.2.

1 Introduction

A research for the next generation supersonic transport named NEXST (National Experimental Supersonic Transport) program had been advanced in JAXA (Japan Aerospace Exploration Agency) [1]. One of main activities of the NEXST program was to develop of an optimum aerodynamic design technology. A target of the aerodynamic design was set to the drag reduction on the supersonic cruise condition, a small scaled and non-powered supersonic experimental airplane (NEXST-1) was designed using a CFD based inverse design method with four design concepts for the drag reduction [2].

A supersonic flight test using the NEXST-1 is planned to validate the aerodynamic design concepts and design process at high Reynolds number conditions. The flight test was successfully conducted on October 2005 at Woomera test range in Australia [3], and aerodynamic data could be obtained from the supersonic regions to the low-speed regions. The aerodynamic design concepts and design process can be confirmed by the flight test at the supersonic cruise condition M=2.0 [4-7]. On the other hand, the flight test results at transonic regions are interested to validate the CFD solver. In general, the flow field around the SST configurations at the transonic region is more complex than the supersonic region. Therefore, the comparisons with CFD results and flight test results are very valuable to validate the CFD analysis at high Reynolds number and transonic region.

In this paper, CFD results at the transonic regions were validated using the flight test results. Furthermore, CFD results at low Reynolds number conditions were also validated using wind tunnel test results.

2 Aerodynamic Design

A target of the flight conditions for the aerodynamic design of the NEXST-1 was set to a design point as the lift coefficient C_L=0.1, Mach number M=2.0 and altitude H=18km that

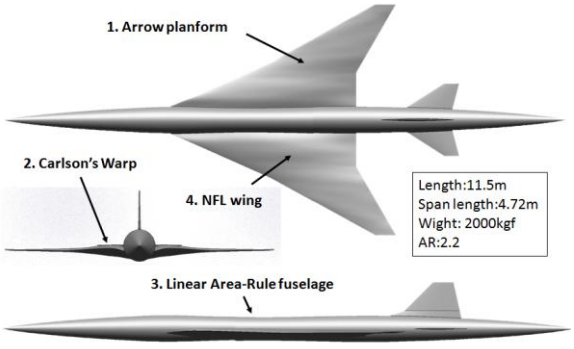

Fig. 1 Schematics of the NEXST-1configuration

was a supposed cruise condition of the SST. To reduce the drag at the design point, four drag reduction concepts were applied to the aerodynamic design of the NEXST-1. 1) cranked arrow wing planform, 2) warped wing, 3) area ruled fuselage and 4) natural laminar flow (NLF) wing can reduce the supersonic drag components (the lift dependent drag, the wave drag and the friction drag). The CFD based inversed design method was used to derive an optimum geometry of the NEXST-1. Details of the aerodynamic design process were reported on reference 2. Figure 1 shows the geometry of the NEXST-1. Benefits of each design concepts were confirmed by the CFD analysis and wind tunnel tests. And then, validation of the design tools was confirmed at high *Re* conditions from the flight test.

3 Aerodynamic Force Measurements

Three kinds of aerodynamic data can be obtained from the flight test, CFD analysis and wind tunnel tests. Measurement details of these data were shortly mentioned in this chapter.

3.1 Flight Test

Figure 2 shows the overall flight test plan using the NEXST-1. Although, the objective of the flight test was validation of the design concepts and design process at the design point (M=2.0), aerodynamic forces were obtained at the transonic and subsonic region. Figure 3 shows the flight path of the flight test. The circle symbols plotted on Fig.3 are corresponded to evaluation data points. At transonic region (called as transonic and recovery phase), aerodynamic data at only a point was obtained at each Mach numbers. Because influences of the unsteady flow want to eliminate from flight test results, those evaluation points at the transonic region were selected to the data that has not abrupt change of the airplane attitude and control surface deflections. Table 1 shows the detail flight conditions at the each evaluation point at the supersonic and transonic regions. Reynolds numbers based on the mean aerodynamic chord

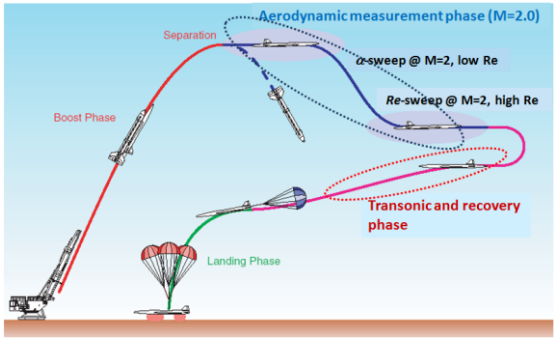

Fig.2 Overall flight test plane of the NEXST-1

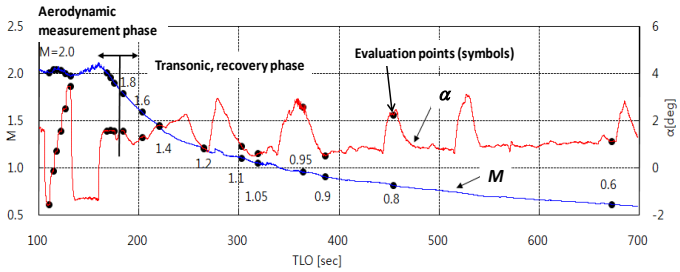

Fig.3 Flight path at supersonic and transonic phase

phase		step No./ target M_∞	T_{LO} [sec]	M_∞	α [deg]	Q [kPa]	H [km]	Re[×10^6] based on MAC
Aero. Measure. Phase (design points)	α-sweep phase	α_1	110.22	2.00	-1.57	18.19	18.94	12.72
		α_2	114.22	2.04	-0.14	18.85	18.91	13.37
		α_3	117.72	2.04	0.71	20.18	18.51	14.25
		α_4	121.92	2.03	1.53	21.30	18.10	14.93
		α_5	126.43	2.00	2.51	22.08	17.68	15.54
		α_6	131.25	1.97	3.44	22.15	17.47	15.84
	Re-sweep phase	Re_1	167.35	2.01	1.56	52.59	12.24	34.25
		Re_5	171.35	1.96	1.58	54.44	11.69	35.15
		Re_9	175.33	1.90	1.56	53.18	11.45	34.70
transonic, recovery phase		1.8	184.10	1.79	1.56	45.57	11.68	31.62
		1.6	203.20	1.59	1.29	31.07	12.58	25.31
		1.4	220.18	1.44	1.80	24.20	12.91	21.94
		1.2	264.28	1.21	0.81	19.08	12.21	20.33
		1.1	302.36	1.10	0.90	19.31	10.98	21.58
		1.05	318.34	1.05	0.58	18.78	10.53	21.70
		0.95	363.48	0.95	2.55	19.75	8.90	24.11
		0.9	386.21	0.90	0.51	18.99	8.42	24.11
		0.8	454.01	0.81	2.24	19.40	6.78	26.20
		0.6	672.00	0.61	1.10	19.65	2.44	30.39

Table 1 Air data at the flight test

length at the transonic region are 20.3 – 26.2 x 10^6.

Aerodynamic forces on the flight test were measured by the IMU sensor (Inertial Measurement Unit) located at the gravity center of the NEXST-1. Detail configuration of the NEXST-1 on the flight test was not corresponded to the configuration on CFD analysis. Because, a Pitot probe and a total temperature sensor (TAT), etc.(called as additional parts) were installed to the NEXST-1 at the flight test. Furthermore, the control surfaces were deflected at the flight test, and structure of the airplane was deformed by aero-elastic effects [8-10]. To compare with CFD results, the configuration of the NEXST-1 at the

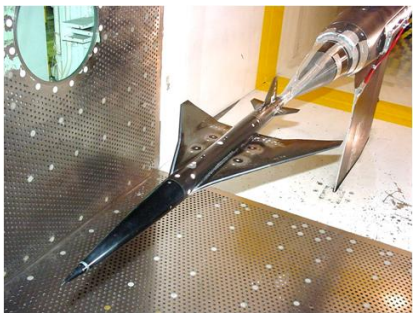

Fig.4 JAXA 2m x 2m transonic wind tunnel

flight test has to correspond with the configuration at the CFD analysis. The aerodynamic effects of the additional parts were compensated at the CFD analysis. Aerodynamic data obtained from the flight test were corrected as the configuration with no deflection of the control surfaces. Further, the angles of attack α measured by the Pitot probe were corrected by the aero-elastic analysis of the NEXST-1 [10]. Because the Pitot probe was installed near the airplane nose that deformed by acceleration of the airplane.

3.2 CFD Analysis

The CFD analysis was performed using the structured mesh code UPACS (Unified Platform for Aerospace Computation Simulation) developed by JAXA. The Navier-Stokes flow solver is based on a cell-centered finite volume method. The Splart-Allmaras one equation model is used to simulate turbulent flow in UPACS code. Detail of the CFD code was described in reference 8,9.

CFD analysis were conducted on a clean configuration without the Pitot probe and TAT sensor at the flight test conditions (high *Re*, see table1) and wind tunnel test conditions (Low *Re*). Some additional parts had been installed to the NEXST-1. This complex geometry is not suitable for the computation using UPACS code, because the UPACS code has the structure mesh system. Therefore, effects of additional parts were cleared by the CFD analysis using the unstructured mesh code named TAS code (Tohoku University Aerodynamic Simulation). Effects of additional parts were also confirmed by the wind tunnel test. Additional parts induce to the increment of drag component [8,9].

3.3 Wind Tunnel Tests

Wind tunnel tests were conducted at 2m x 2m JAXA transonic wind tunnel (Fig.4). Two wind tunnel test models with 8.5% scale of the NEXST-1 were used separately for the force measurement and surface pressure measurement. Reynolds number based on the mean aerodynamic chord length is Re=2.6 x 10^6. A tape type roughness was attached on the wing leading-edge to promote the boundary layer transition near the leading edge of the wing. Because, wind tunnel test condition should correspond to the conditions of CFD analysis that has fully turbulent model.

4 Results and Discussion

4.1 Comparison with Wind Tunnel Test

At first, CFD results were compared with the wind tunnel results at low *Re* conditions (Re=2.6 x 10^6). As mentioned before, CFD analyses were conducted at same *Re* with the wind tunnel tests. Figure 5 shows C_L-α characteristics at several *M*. The CFD results were revealed good agreement with the wind tunnel test results at M=1.2, 1.05. However, slight difference on both results were observed at M=0.95, 0.8.

$$C_D = K(C_L - C_{L0})^2 + C_{Dmin} \qquad (1)$$

To break down the C_L-C_D characteristics, the C_D represents as a second order of the C_L (Eq.1). Figure 7 shows variation of the K, C_{L0} and C_{Dmin} at the transonic region. Value of the K is depended on the wing planform. Variation of the K value by CFD analysis is agreed with that by the wind tunnel tests. The C_{L0} shows the different trend on both results. The C_{L0} of wind tunnel test are larger than the CFD results at the subsonic region (M<1.0), however, the C_{L0} of wind tunnel test are smaller than the CFD results at the supersonic region (M>1.0). In general, the value of the C_{L0} means the strength of the warp wing. It was suggested that the difference of the C_{L0} by CFD and wind tunnel test were induced to the difference of the spanwise load distributions. Therefore, it was suggested that the different C_P distributions will

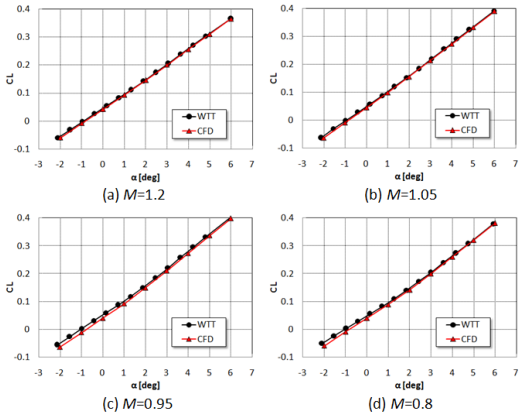

Fig.5 Comparison of CFD results with wind tunnel test results (C_L-a characteristics, Re=2.6x10^6)

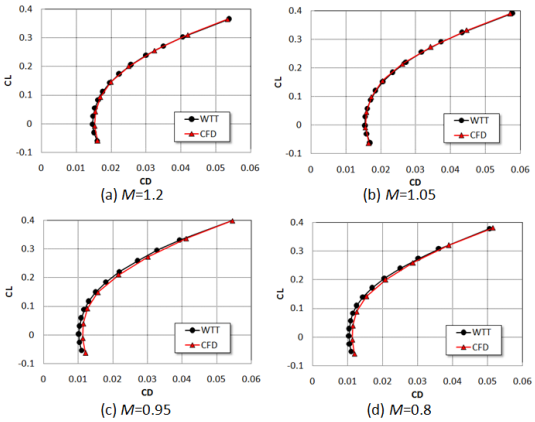

Fig.6 Comparison of CFD results with wind tunnel test results (C_L- C_D characteristics, Re=2.6x10^6)

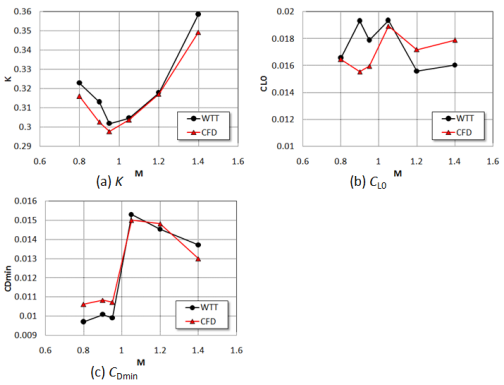

Fig.7 C_L- C_D characteristics by CFD and wind tunnel test results (Re=2.6x10^6)

be observed on both results. Figure 8 shows static pressure coefficient C_P distributions at the spanwise location η=0.3, 0.7 on α=0deg. However, C_P distributions by the CFD were relatively corresponded with the wind tunnel test results. It means that the different of aerodynamic forces observed in Fig.5 was not observed on C_P distributions in Fig.8. Good agreements were observed on the C_{Dmin} at the

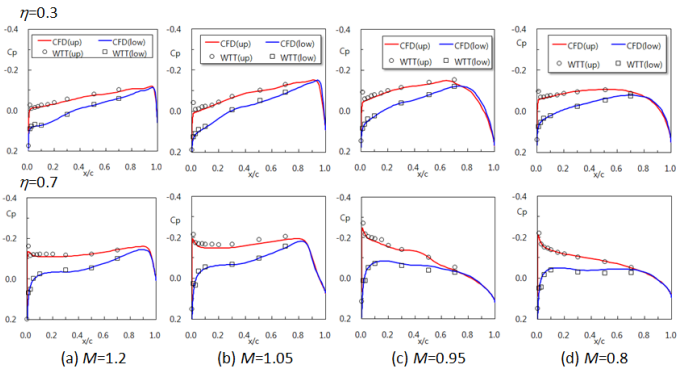

Fig.8 C_P distributions by CFD and wind tunnel test (α=0deg, Re=2.6x10^6)

supersonic region, while the values of the C_{Dmin} of wind tunnel results are smaller than the CFD results at the subsonic region.

4.2 Reynolds number effects in CFD

CFD results at the flight test conditions (high Re; see table1) were compared with the CFD results at wind tunnel test conditions (Low Re). Figure 9 shows C_L, C_D, C_m characteristics at M=1.05. C_L-α (Fig.9(a)), C_m-α (Fig.9(c)) characteristics shows good agreement on both results. However, the C_D at wind tunnel test conditions was larger than that at flight test conditions. These differences of C_D values on both results were not changed at several angles of attack. When the drag was broken down to the pressure drag and friction drag component, it was cleared that the difference of the drag on both results was induced by the different value of the friction drag component. Figure 10 shows the difference of C_D values obtained from the

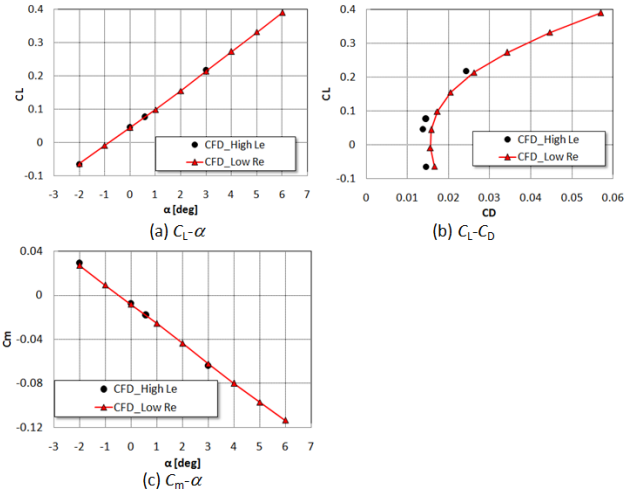

Fig.9 CFD results at different Re (M=1.05)

CFD analysis at both *Re*. Values of the friction drag correction obtained from Plantle-Hoerner's method [11] were also plotted in Fig.10. Similar trend were observed on both curves. However, Plantle-Hoerner's method for correction of the friction drag depended on the *Re* was slightly larger than the values obtained by the CFD analysis using Splart-Allmaras turbulent model.

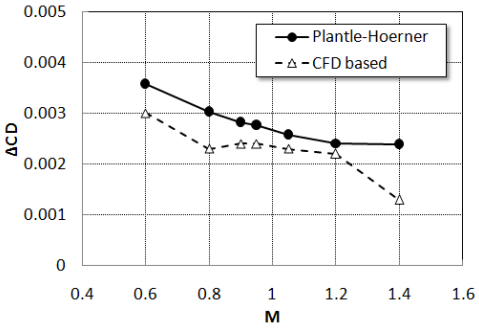

Fig.10 Values of the drag correction at different Reynolds number

4.3 Comparison with Flight Test

To validate the CFD analysis at high *Re*, CFD results were compared with the flight test results. C_L-α characteristics obtained from the flight test and CFD were seen on Fig.11. As mentioned before, a data at one angle of attack was obtained at each *M* from the flight test (see table 2). However, CFD analyses were conducted at four α points at same *Re* and *M* with the flight test conditions. C_L from the flight test was slightly larger than the C_L by CFD analysis. Figure 12 shows C_L - C_D curves at several *M*. The C_D from the flight test were smaller than the CFD results at *M*=1.2, 1.05. Figure 13 shows C_m-α characteristics as Fig. 11, 12. The C_m from the flight test show relatively good agreement with CFD results.

Figure 14 shows C_L -α, C_L - C_D curve at *M*=2.0 (the design point of the NEXST-1) [7,8]. At *M*=2.0, the aerodynamic data at several α were obtained at same *M*, *Re*. CFD analysis at *M*=2.0 were considered the friction drag corrections using the boundary layer transition location obtained from the flight test [8,12]. Locations of the boundary layer transition depend on the pressure distributions and *Re*. Surface static pressure distributions C_P depend on the α and *M*. The *Re* and *M* is different at the transonic region and *M*=2.0, however C_P

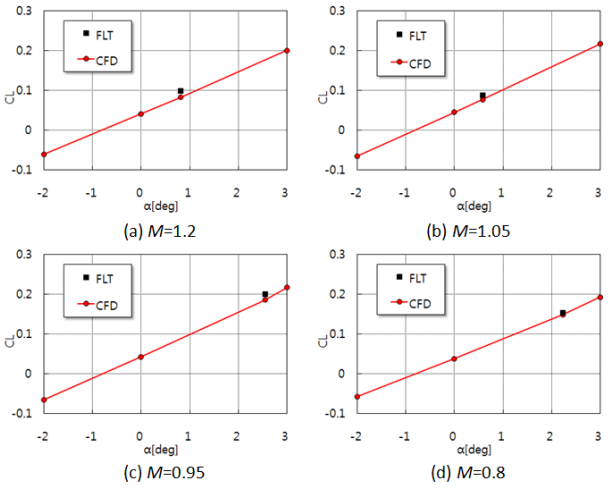

Fig.11 Comparison of CFD results with flight test results (C_L-*a* characteristics, *Re*=20.3-26.2x10^6)

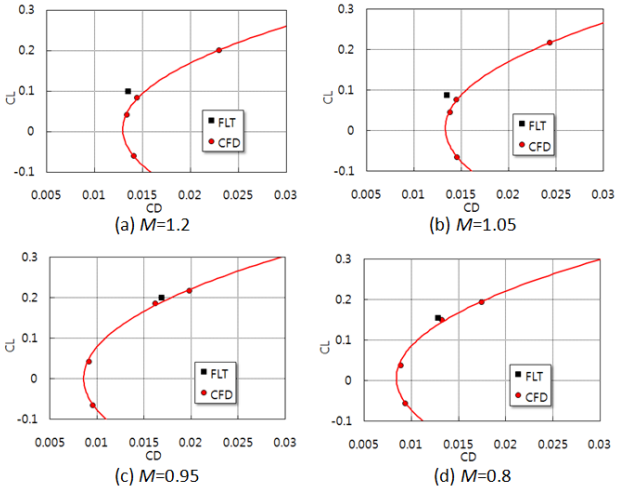

Fig.12 Comparison of CFD results with flight test results (C_L- C_D characteristics, *Re*=20.3-26.2x10^6)

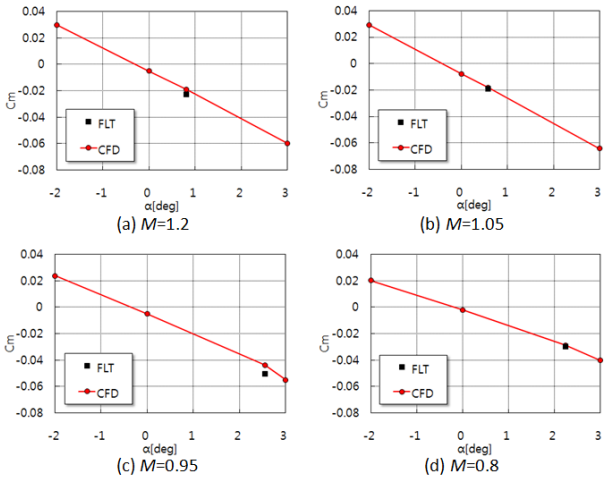

Fig.13 Comparison of CFD results with flight test results (C_m- *a* characteristics, *Re*=20.3-26.2x10^6)

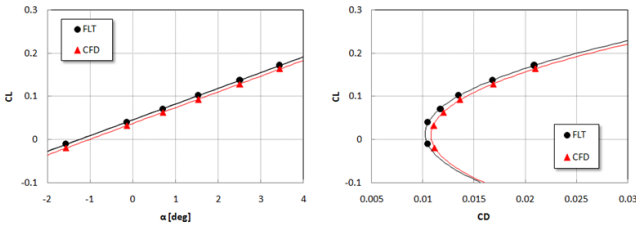

(a) C_L-a (b) C_L- C_D

Fig.14 Comparison of CFD results with flight test results at the design point (M=2.0, Re=12.7-15.8x10^6)

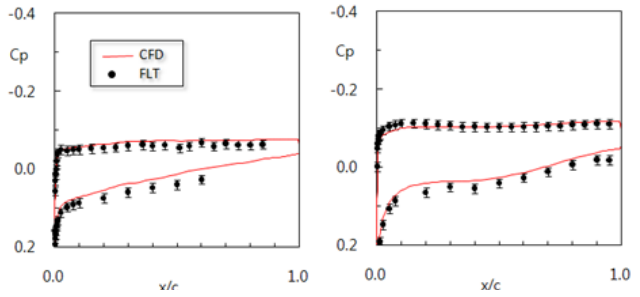

(a) η=0.3 (b) η=0.7

Fig.15 C_P distributions by CFD and flight test results at the design point (α=1.53deg, M=2.0, Re=12.7-15.8x10^6)

distributions at α=0.81deg (M=1.2) are similar with C_P distributions at the design point (Fig.15 and Fig.8 (a)). It means that C_P distributions at M=1.2 were similar with C_P distributions at the design point that can be delayed the boundary layer transition. Because, C_P distributions at the design point were the optimum C_P distributions for the natural laminar flow wing [2]. Therefore, it was suggested that the laminar region on the upper surface of the wing was exist at M=1.2 of the flight test. This delay of the transition at the flight test can reduce drag than the CFD results obtained from fully turbulent analysis.

Figure 16 shows the minimum drag at the several M. The C_L - C_D curves obtained by the CFD analysis were approximated by Eq.1. The C_{Dmin} at the flight test were obtained by an assumption that the C_L - C_D curve at the flight test has same value of the K and C_{L0} of the CFD results. It means that the C_L - C_D curves of the CFD results shift along x-axis as left figure on Fig.16 until the flight test results located on a line of the shifted C_L - C_D curve. The value of the shift from CFD result to the flight test results is the difference of the C_{Dmin} on the CFD and flight test results. Wind tunnel test results at high Re were also estimated by Re correction using CFD results at the wind tunnel test Re and the flight test Re (see Fig.9). When M increases upto M=0.95, C_{Dmin} at M=0.6, 0.8, 0.9 doesn't change obviously, however slightly increases at M=0.95. Over M=1.0 regions, the C_{Dmin} increases drastically at M=1.05. And then, the C_{Dmin} decreases linearly with increasing M upto 1.8. This variation of the C_{Dmin} at the transonic region is similar with the drag variations observed at the conventional aircraft. Similar trend of C_{Dmin} characteristics was observed from the results by the CFD analysis. However, as mentioned before, values of the flight test results were smaller than the CFD analysis. The difference of the C_{Dmin} at M=1.05 – 1.4 were larger than the difference at other M. On the other hand, wind tunnel test results were well agreed with the flight test results at the subsonic regions (M<1), but relatively good agreement with the CFD results were observed at supersonic regions (M>1).

When CFD results were compared with the flight test results, C_L, C_m characteristics were relatively corresponded on both results. However, the C_D from the CFD results was larger than the flight test results at wide transonic regions. Similar trend was also observed results at M=2.0. The reason of the different were not cleared in this paper, further inspection and analysis should be conducted to validate the CFD analysis at the transonic region. However, the variations of C_D along M-sweep obtained by the CFD analysis were corresponded to the flight test results.

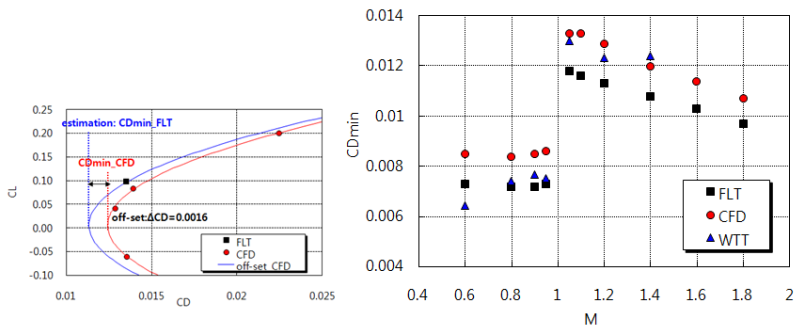

Fig.16 C_{Dmin} estimation at transonic regions (Re=20.3-26.2x10^6)

5 Conclusion

Results of CFD analysis on the SST configuration at transonic region were validated by comparing with NEXST-1 flight test and wind tunnel tests.

- When CFD results were compared with wind tunnel test results at Re=2.6x10^6, good agreement were observed at M>1, relatively poor agreement were observed on low α at M<1.
- From CFD results at different Re, the difference of the friction drag component was main reason of difference of the total drag.
- When CFD results were compared with the flight test results at Re=20.3-26.2x10^6, difference of the drag component were observed on both results. Further data analysis is needed to clear the difference. However, similar trend were obtained on both results.

Acknowledgements

The authors gratefully acknowledge to the staff of Mitsubishi Heavy Industries, Ltd., Kawasaki Heavy Industries, Ltd. and Fuji Heavy Industries, Ltd. for their contribution of the flight test of the NEXST-1. The authors also thank to Mr. Nakahata, K. and Mr. Noguchi, M. for their helpful support on the flight test analysis and the wind tunnel tests.

References

[1] Ohnuki, T., Hirako, K., Sakata, K. National Experimental Supersonic Transport Project, *Proceedings of 25th Congress of the International Council of the Aeronautical Sciences*, ICAS Paper 2006-1.4.1.

[2] Yoshida, K., and Makino, Y. Aerodynamic Design of Unmanned and Scaled Supersonic Experimental Airplane in Japan, *ECCOMAS 2004*, Jyväskylä/Finland, July, 2004.

[3] Fujiwara, T., Hirako, K., Ohnuki, T. Flight Plan and Flight Test Results of Experimental SST Vehicle NEXST-1, *Proceedings of 25th Congress of the International Council of the Aeronautical Sciences*, ICAS Paper 2006-6.2.1.

[4] Tokugawa, N., Kwak, D.Y., Yoshida, K. Transition Measurement System of Experimental Supersonic Transport "NEXST-1", *Proceedings of 25th Congress of the International Council of the Aeronautical Sciences*, ICAS Paper 2006-3.3.2.

[5] Kwak, D.Y., Yoshida, K., Ishikwa, H., Noguchi, M. Flight Test Measurements of Surface Pressure on Unmanned Scaled Supersonic Experimental Airplane, AIAA Paper 2006 -3483.

[6] Tokugawa, N. and Yoshida, K. Transition Detection on Supersonic Natural Laminar Flow Wing in the Flight, AIAA Paper 2006 -3165.

[7] Kwak, D.Y., Tokugawa, N., Yoshida, K. Demonstration of Aerodynamic Design Technologies on Supersonic Experimental Airplane (NEXST-1) by Flight Test, *Proceedings of 2006 KSAS-JSASS Joint International Symposium on Aerospace Engineering*, 2006, pp.176-182, 2006.

[8] Ishikawa, H., Kwak, D.Y., Yoshida, K. CFD Analysis on Flight Test Results of Supersonic Experimental Airplane NEXST-1, AIAA Paper 2007-3925.

[9] Ishikawa, H., Kwak, D.Y., Yoshida, K. Computational Fluid Dynamic Analysis on Flight Test Results of Supersonic Experimental Airplane NEXST-1, Jour. of Aircraft, submitted.

[10] Kawakami, H., Takatoya, T., Ishikawa, H. Static Aeroelastic Analysis of Supersonic Experimental Airplane NEXST-1 Flight Test," AIAA Paper 2007-4174.

[11] Air Force Flight Dynamics Laboratory USAF, Stability and Control, DATCOM, 1975.

[12] Tokugawa, N., Kwak, D.Y., Yoshida, K. and Ueda, Y, Transition Measurement of Natural Laminar Flow Wing on Supersonic Experimental Airplane (NEXST-1), Jour. of Aircraft, submitted.

Copyright Statement